First-principles characterization of Ni diffusion kinetics in β-NiAl

Kristen A. Marino[1] and Emily A. Carter[2]
[1]*Department of Chemical Engineering, Princeton University, Princeton, New Jersey 08544-5263, USA*
[2]*Department of Mechanical and Aerospace Engineering and Program in Applied and Computational Mathematics, Princeton University, Princeton, New Jersey 08544-5263, USA*

(Received 17 March 2008; revised manuscript received 3 August 2008; published 11 November 2008)

First-principles density functional theory calculations are performed to examine five postulated diffusion mechanisms for Ni in NiAl: next-nearest-neighbor (NNN) jumps, the triple defect mechanism, and three variants of the six-jump cycle. In contrast to most previous theoretical work, which employed empirical interatomic potentials, we provide a more accurate nonempirical description of the mechanisms. For each pathway, we calculate the activation energy and the pre-exponential factor for the diffusion constant. Although our quantum mechanics calculations are performed at 0 K, we show that it is critical to include the effect of temperature on the pre-exponential factor. We predict that the triple defect mechanism and [110] six-jump cycle both are likely contributors to Ni diffusion in NiAl since their activation energies and pre-exponential factors are in very good agreement with experimental data. Although the activation energy and pre-exponential factor of NNN jumps agree well with experiment, experimental evidence suggests that this is not a dominant contributor to Ni diffusion. Lastly, the activation energies of the [100] bent and straight six-jump cycles are 1 eV higher than the experimental value, allowing us to exclude both [100] cycle mechanisms.

DOI: 10.1103/PhysRevB.78.184105 PACS number(s): 66.30.Fq, 71.15.Mb, 61.72.J−, 66.30.Ny

I. INTRODUCTION

Modern jet engines operate at temperatures well above the incipient melt temperature of the Ni-based superalloy from which the engine components are made. Component protection from thermomechanical failure is partially provided by thermal barrier coatings (TBCs), which are composed of three parts: a bond coat (BC), a thermally grown oxide (TGO) layer, and a yttria-stabilized zirconia (YSZ) ceramic topcoat. In state-of-the art coatings, the BC is composed of β-(Ni,Pt)Al and acts as a source of Al for the growth of the TGO, alumina (α-Al_2O_3), which grows in between the BC and YSZ. External protection is lost upon spallation of the oxide, leaving the component surface exposed to the harsh conditions in the engine. Improving TBC time to failure is vital to improving engine performance.[1–3]

At the high operating temperatures of the engines, TBCs are constantly evolving due to atomic processes such as diffusion. Since experiments have shown that the presence of Pt prevents the formation of brittle, fast-growing Ni-rich oxides[1] one possible role for Pt is to enhance Al diffusion to the BC/TGO interface to favor Al_2O_3 rather than $NiAl_2O_4$ formation, thereby delaying spallation. Al diffusion cannot be studied experimentally due to a lack of a suitable isotope, but Ni diffusion in single-crystal NiAl has been measured.[4] While our interest ultimately lies in characterizing Al diffusion, a logical first step is to study Ni diffusion, with which we can quantify any errors in our approach before examining Al diffusion in NiAl. As it turns out, multiple mechanisms have been proposed for Ni diffusion, but controversy remains as to which is the dominant mechanism. No comprehensive first-principles investigation of all postulated Ni diffusion mechanisms has been reported. Here we present such a study, with the aim to provide some clarity by confirming or ruling out various proposed mechanisms.

Atomic diffusion mechanisms in bulk metals involve either vacancies or interstitials. The sizes of Ni and Al atoms dictate that they must diffuse via a vacancy mechanism since they are not small enough to pass through interstitial sites. Diffusion rates are characterized by the diffusion constant, D, which exhibits an Arrhenius temperature dependence [Eq. (1)],

$$D = D_0 e^{(-Q/k_B T)}. \tag{1}$$

The activation energy, Q, and pre-exponential factor, D_0, are constants for a given diffusion path, where Q is not only the activation barrier to migration, but in the case of vacancy-controlled diffusion, Q is the sum of the vacancy formation energy and migration activation barrier. Vacancy-mediated diffusion requires prior thermally activated formation of a vacancy, so one must consider the energy cost of forming a defect (E_d) in perfect stoichiometric NiAl with no constitutional defects (by contrast, nonstoichiometric NiAl has defects present initially) in addition to the energy barrier for the atoms to move from one point to another (E_m) to obtain the overall activation energy. As we shall see, all postulated mechanisms start with either a Ni vacancy or cluster of defects that include Ni vacancies.

The earliest isotope experiments on Ni diffusion were performed by Hancock and McDonnell,[5] who examined Ni diffusivity as a function of NiAl stoichiometry (48.3–58.7 at. % Ni) in polycrystalline alloys. Their results showed that the rate of diffusion was highly dependent on composition. The alloy with the slowest rate of diffusion (and hence maximum activation energy) had a composition slightly off the stoichiometry at ~49.5 at. % Ni. The diffusion rates increased as the alloy became more Ni-rich or Al-rich.[5] Later, Frank *et al.*[4] used the ^{63}Ni isotope and secondary-ion mass spectrometry to study diffusion in single-crystal alloys with a range of Ni concentrations from 46.8 to 56.6 at. % over a temperature range of 1050–1630 K. By contrast to the earlier work, no minimum was found on a plot of the diffusion coefficient with respect to alloy

composition; in fact, the activation energy was nearly constant (~3 eV) for the 46.5–53 at. % Ni alloys. Frank *et al.*[4] did find that the diffusion rate increased as the Ni concentration increased beyond stoichiometric. The discrepancy between the results of Frank *et al.*[4] and Hancock and McDonnell[5] for Al-rich alloys is likely due to the presence of grain boundaries in Hancock and McDonnell's polycrystalline samples.[5] Frank *et al.*[4] postulated that the triple defect mechanism (*vide infra*) must be the dominant mechanism of Ni diffusion since the presence of constitutional Ni vacancies did not lead to increased diffusion in Al-rich NiAl.

Since current experimental probes lack the spatial and time resolution to determine the atomic level mechanism of Ni diffusion in NiAl, numerous simulations have been performed, reaching diverse conclusions as to the dominant mechanism. Divinski and Herzig[6] calculated diffusion constants for the six-jump-cycle mechanism (*vide infra*) using molecular statics with embedded atom method (EAM) potentials and Monte Carlo simulations. While the activation energy and diffusion constant of the six-jump cycle in the [110] direction agreed well with experiment, their simulations indicated that this mechanism would only contribute to Ni diffusion at $T \leq 1100$ K. With the same methodology, Divinski *et al.*[7] concluded that the triple defect mechanism is the dominant mechanism of Ni diffusion for Al-rich, stoichiometric, and slightly Ni-rich (≤52 at. % Ni) NiAl, while the antistructure bridge (ASB) mechanism also operates in alloys with high Ni contents (≥55 at. %). Chen *et al.*[8] also concluded that the triple defect mechanism was the dominant mechanism using molecular dynamics (MD) with a modified analytic EAM potential to calculate the activation energies of next-nearest-neighbor (NNN) Ni jumps, the triple defect mechanism, and the six-jump cycle. However, using molecular dynamics with EAM potentials, Soule de Bas and Farkas[9] observed that the [110] six-jump cycle was the dominant diffusion mechanism in NiAl. The six-jump cycle was also studied by Mishin *et al.*[10] using molecular statics with EAM potentials after confirming the validity of their potential by calculating the migration energy of a NNN jump with first-principles techniques. They predicted that the [110] six-jump cycle would dominate over a similar mechanism in which the Ni atom would move in the [100] direction but that the diffusion rate of NNN Ni jumps was high enough that the latter also could occur. Recently, Xu and Van der Ven[11] calculated migration energies of several jumps using first-principles techniques but did not calculate diffusion coefficients.

In this work, we use first-principles quantum mechanics calculations to calculate activation energies and diffusion constants for the five previously proposed Ni diffusion mechanisms: NNN jumps, the triple defect mechanism, and three variants of the six-jump cycle to clarify which possible mechanisms for Ni diffusion are truly viable. Moreover, since no measurements have been made for Al diffusion in NiAl, as we shall see, our work can be used as a basis for beginning to understand Al diffusion in NiAl as well.

II. THEORETICAL METHODS

A. Calculational details

The Vienna *ab initio* simulation package (VASP) (Refs. 12 and 13) is used to perform spin-polarized density functional theory (DFT) (Refs. 14 and 15) calculations with a plane-wave basis set. Electron exchange and correlation is described within the generalized gradient approximation (GGA) using Perdew-Burke-Ernzerhof (PBE) functionals,[16,17] and the interactions of the valence electrons with the core electrons and nuclei are represented by projector augmented wave (PAW) potentials, which are all-electron potentials within a frozen-core approximation.[18,19] As required for metals, partial band occupancies are set by the first-order Methfessel-Paxton method.[20] A Fermi smearing width of 0.2 eV is sufficient to keep entropy terms less than 1 meV/atom. The kinetic-energy cutoff for the plane-wave basis set is converged at 350 eV, given that decreasing the cutoff to 300 eV or increasing the cutoff to 400 eV changed the total energy by 1 meV/atom or less.

Bulk NiAl adopts a B2 structure, which consists of two interpenetrating simple-cubic lattices. The unit cell consists of two atoms, but as described below converged results for isolated defects require 54- and 128-lattice site cells. The number of k points is converged for all supercell sizes considered, and k-point sampling utilizes Monkhorst-Pack grids.[21] k-point convergence is considered to be achieved when increasing the k-point grid by two in each direction causes a total-energy change of 1 meV/atom or less. As a result, $6\times6\times6$ and $4\times4\times4$ grids are used for the 54- and 128-lattice site cells, respectively.

The equilibrium lattice parameter of NiAl is determined by calculating the energy of unit cells with volumes ±5% of the experimentally determined value, which are then fit to Murnaghan's equation of state.[22] This bulk lattice parameter is used for all subsequent calculations and is not permitted to change in order to mimic a bulk crystal with a small concentration of defects. In order to eliminate artificial defect-defect interactions due to periodic images, converged cell sizes have to be determined. This is done by calculating the defect formation energy using supercells of increasing size (54, 128, and 250 lattice sites). Once the defect formation energy no longer changes (to within 0.05 eV) as the number of atoms in the cell increases, the cell size is deemed adequate for studying diffusion events representative of mechanisms occurring in the bulk. Thus, a 54-lattice site cell is used for studying the next-nearest-neighbor jump and six-jump cycle mechanisms, while a 128-lattice site cell is required for the triple defect mechanism calculations. In our work, the smallest distance between a point defect in a defect cluster to the closest point defect in a periodically replicated defect is twice the lattice constant (here ~5.8 Å). In the bulk lattice, the NN and NNN distances are 2.5 and 2.9 Å. Further, the migration energies of step II of the [110] six-jump cycle mechanism were calculated to be 0.54 eV in a 127-atom cell and 0.56 eV in a 53-atom cell. The 0.02 eV decrease in energy when increasing the number of atoms in the cell is within the expected uncertainty of the calculations. For all calculations, the atomic positions are permitted to relax according to a conjugate gradient or quasi-Newton algorithm until the forces on each atom are less than 0.01 eV/Å.

B. Calculating diffusion coefficients

For metals held far below their melting temperature, the atomic positions do not deviate greatly from their equilib-

rium positions. In this case, it is reasonable to invoke the harmonic approximation to transition state theory (hTST) to estimate rate constants. The harmonic transition state theory rate constant, expressed as[23]

$$k^{\mathrm{hTST}} = \nu_0 e^{-(E_m/k_B T)} = \frac{\prod_i^{3N} \nu_i^{\mathrm{initial}}}{\prod_i^{3N-1} \nu_i^{\mathrm{saddle}}} e^{-(E_m/k_B T)}, \quad (2)$$

where ν_i is a normal mode frequency and E_m is the migration energy barrier, can be determined using a two-step approach. First, the minimum energy path (MEP) is determined to calculate E_m. Then the normal mode frequencies, ν_i, at the initial state and saddle point are calculated.

The climbing image nudged elastic band (CINEB) method[24] can be used to find the MEP of atomic migration when both the initial and final minima are known. The diffusion process is initially represented by a series of images constructed by a linear interpolation of the atomic positions between the initial and final states. The images are strung together by a "band," which is permitted to relax until the forces on the images reach a specified threshold, after which the highest energy image is allowed to "climb" up the MEP to the highest energy point of the MEP, which is the saddle point. The difference in energy of the saddle point and initial minimum is the migration (activation) energy, E_m. Due to the large masses of the atoms involved, we can safely neglect zero-point energy corrections to E_m.

The normal mode frequencies are related to the eigenvalues of the Hessian, the matrix of second derivatives of the energy with respect to position. Here the Hessian is constructed from finite differences of analytic gradients, in which all atoms that are within 4 Å of the diffusing atom anywhere along the MEP are displaced ±0.02 Å to evaluate forces. The cutoff distance is selected by calculating the frequencies using an increasing number of atoms. We first considered only the NN atoms to the migrating atom and then all the NN and NNN atoms. The ratio ν_0 found using the NN and NNN atoms was five times larger than the ratio using only the NN atoms, suggesting it is imperative to use all neighbors up through NNN. Due to the expense of the calculations, we could not go beyond NNNs. (The number of atoms included in calculating these Hessians ranged from 22 to 30.) All of the NN and NNN atoms were found to lie within 4 Å of the diffusing atom at any point along the path, hence the choice of cutoff radius. We verify the robustness of the frequencies calculates at displacements of ±0.02 Å by also using ±0.03 Å displacements, which left the frequencies unchanged to within 1 cm^{-1}. The number of imaginary frequencies calculated is indicative of the nature of the critical point on the potential-energy surface. A local minimum has no imaginary frequencies, while a transition state has one and high order saddle points have at least two. If the magnitude of the imaginary frequency at the saddle point was less than 100 cm^{-1}, the displacement was increased to ±0.03 Å to ensure we are capturing the true nature of the potential energy surface at that point.

The expression for the diffusion constant given in Eq. (1) is an empirical one. A more detailed theoretical expression is necessary to relate results from our constant volume, 0 K calculations to experimental data at high temperatures. Consider the three-dimensional random-walk problem, where the diffusion constant is a function of the jump rate Γ,[25]

$$D = \frac{1}{6} a^2 \Gamma. \quad (3)$$

The factor 1/6 arises since diffusion in a three-dimensional lattice can occur in both the positive and negative x, y, and z directions, so motion along any one direction on average is 1/6 of the sum of diffusion in all six directions. Here a represents the jump distance. The jump rate is typically expressed as a function of the free energy barrier, $\Delta G^{\ddagger}$, which can in turn be expressed in terms of entropic and enthalpic barriers, $\Delta S^{\ddagger}$ and $\Delta H^{\ddagger}$, respectively,

$$\Gamma = \nu e^{(-\Delta G^{\ddagger}/k_B T)} = \nu e^{(\Delta S^{\ddagger}/k_B)} e^{(-\Delta H^{\ddagger}/k_B T)} \approx \nu e^{(-Q/k_B T)}. \quad (4)$$

Here ν is a pre-exponential factor for which an expression will be derived below. Under typical experimental conditions, the entropic barrier $\Delta S^{\ddagger}$ is usually negligible and therefore the activation energy Q is taken to be the enthalpic barrier, $\Delta H^{\ddagger}$, leaving ν as the only unknown. The diffusion constant in Eq. (3) is then expressed as

$$D = \frac{1}{6} a^2 \nu e^{(-Q/k_B T)}. \quad (5)$$

The goal of the following derivation is to find a theoretical expression for ν. Using statistical mechanics, Vineyard[23] derived Eq. (6), which relates the jump rate to the internal energy barrier $\Delta U^{\ddagger}$,

$$\Gamma = \nu^* e^{(-\Delta U^{\ddagger}/k_B T)}. \quad (6)$$

Vineyard[23] showed that $\nu^* = \nu_0$ of Eq. (2) when the harmonic approximation is made at finite T. However, our calculations are carried out at 0 K under constant volume, so no thermal expansion of the lattice is accounted for. As a result, the saddle-point structure found by the CINEB algorithm is compressed[10] compared to the lattice at 1200–1500 K, the temperature range for which experimental data were collected. For situations in which the diffusing atom does not cause large distortions in the lattice as it moves, the compression will be negligible, and ν_0 at 0 K will be essentially equivalent to the frequency ratio at high temperatures. However, when the diffusing atom is large and distorts the lattice as it moves, the more compressed the lattice and the slower the rate of atomic motion. The calculated vibrational frequencies at the saddle point are then too large, resulting in a calculated pre-exponential factor which is too small. In this case, the entropic barrier cannot be ignored. Instead, we equate the jump rates in Eqs. (4) and (6),

$$\Gamma = \nu e^{(\Delta S^{\ddagger}/k_B)} e^{(-\Delta H^{\ddagger}/k_B T)} = \nu^* e^{(-\Delta U^{\ddagger}/k_B T)} \cong \nu_0 e^{(-\Delta U^{\ddagger}/k_B T)}, \quad (7)$$

where the last equality is due to Vineyard.[23] Our calculations are carried out at constant volume, and therefore the enthal-

pic barrier $\Delta H^{\ddagger}=\Delta U^{\ddagger}+p\Delta V^{\ddagger}$ is equal to the internal energy barrier $\Delta U^{\ddagger}$. As a result, Eq. (7) simplifies to $\nu e^{(\Delta S^{\ddagger}/k_B)}=\nu_0$ or $\nu=\nu_0 e^{(-\Delta S^{\ddagger}/k_B)}$. Since the entropic barrier at high temperatures is negligible, we see that $\nu_0 e^{(-\Delta S^{\ddagger}/k_B)}$ at 0 K should be approximately equal to the measured ν_0 at high temperatures. The calculated diffusion constant now can be written as in Eq. (1), where the term in parentheses is the pre-exponential factor,

$$D=\left(\frac{1}{6}a^2\nu_0 e^{(-\Delta S^{\ddagger}/k_B T)}\right)e^{(-Q/k_B T)}. \tag{8}$$

Since we are invoking the harmonic approximation, we can estimate the entropic barrier at 0 K by calculating the vibrational entropy, S_{vib}, of a series of harmonic oscillators at the saddle point and initial minimum. At high temperatures (i.e., $h\nu/k_B T \ll 1$), S_{vib} is expressed as[26,27]

$$S_{\mathrm{vib}}=-k_B\sum_{i}^{3N}\ln\left(\frac{h\nu_i}{k_B T}\right)+3Nk_B. \tag{9}$$

Although N should be equivalent to the number of atoms in the supercell, we have set N to be equal to the number of atoms used to calculate the Hessian for consistency. This approximation amounts to assuming that atoms which are further away will not feel the effects of the diffusing atom and will have the same frequencies at both the minimum and the saddle point. Taking the difference of the two summations will then result in cancellation of these entropic contributions. Since one imaginary frequency is found at the saddle point, the $3N$ in Eq. (9) is replaced by $3N-1$ when calculating the entropy at the saddle point.

The pre-exponential factor in Eq. (8) and the activation energy Q (the sum of the defect formation energy E_d and the migration energy E_m) in Eq. (1) then can be directly compared to experimental data in order to validate our methodology. Calculational details for the defect formation energies presented here were reported earlier[28] but are summarized briefly here. E_d is the formation energy of an alloy with a defect, ΔE_d^f, with respect to the formation energy of the perfect stoichiometric alloy, $\Delta E_{\mathrm{NiAl}}^f$,[29,30]

$$E_d=\frac{\Delta E_d^f-\Delta E_{\mathrm{NiAl}}^f}{x_d}. \tag{10}$$

The value of the defect mole fraction x_d is one divided by the number of atoms in the supercell. The formation energy of an alloy with or without a defect is[29,30]

$$\Delta E_{\mathrm{Ni}_x\mathrm{Al}_{1-x}}^f=E(\mathrm{Ni}_x\mathrm{Al}_{1-x})-xE(\mathrm{Ni})-(1-x)E(\mathrm{Al}). \tag{11}$$

Here the energy of an alloy is referenced as per convention to the energy of the constituent elements in their standard states. Thus E(Ni) and E(Al) are the energy per atom of fcc Ni and Al, $E(\mathrm{Ni}_x\mathrm{Al}_{1-x})$ is the energy of alloy periodic cell with or without defects, and x in Eq. (11) is the number of Ni atoms in the alloy periodic cell.

Other authors[10,30,31] alternatively defined the defect formation energy contributing to the diffusion activation energy, Q, as an effective formation energy, E^{eff}. E^{eff}s have the advantage that they do not rely on reference states, such as the bulk elemental alloys in Eq. (11). Although one could theoretically define the formation energy of an alloy with respect to numerous reference states, the selection of the bulk metals is consistent with the chemistry of alloy formation and is the only appropriate reference state. The equations for these effective formation energies for point defects are derived from the Arrhenius-type concentration dependence of a defect at thermal equilibrium. The formation energy of a point defect is calculated from the formation energies of composition-conserving defect complexes. For example, the formation energy of a $\mathrm{Ni_{Al}}$ is 1/3 of the formation energy, E_{TD}, of a triple defect complex, $\mathrm{Ni_{Al}}+2V_{\mathrm{Ni}}$. However, E_{TD} is calculated from the "raw" formation energies of the individual defects, the difference in energy between a periodic cell with the individual defect minus the energy of a perfect periodic cell. We assert that this is not an appropriate methodology to assess defect formation energies for the diffusion events considered here. First, since all necessary defects must come together for a diffusion event to occur, the interaction between point defects must be accounted for when determining the formation energy of a defect cluster in (Ni,Pt)Al, which is not done when calculating E^{eff}. Although the formation energy of a defect cluster in pure NiAl is approximately the sum of the individual point defect formation energies, we have shown that this is not the case with Pt present.[28] For example, the sum of the individual point defect formation energies comprising a triple defect in NiAl is 1.85 eV, which is very similar to E_d of the interacting triple defect cluster (1.95 eV). By contrast, the same E_d comparison in Pt-doped NiAl reveals very strong defect-defect interactions that cannot be ignored: 0.04 eV for the noninteracting triple defect and 1.32 eV for the interacting triple defect cluster. We have evidence for strong perturbations to the electronic structure of the alloy when Pt is added, even though Ni and Pt have the same valence electronic configuration.[32] Second, the formalism for deriving the effective formation energies depends on setting the formation energy of a Ni antisite atom in Ni-rich NiAl and a Ni vacancy in Al-rich NiAl to zero. While these defects are constitutional defects in the respective alloys (which would have a formation energy of 0 eV at 0 K), it is unreasonable to expect that formation of these point defects as thermal defects would have an energy cost of zero. Therefore, the defect formation energies used to calculate Q in this work are calculated from Eqs. (10) and (11).

While we shall see that vibrational entropy contributes significantly to diffusion coefficient pre-exponential factor, we can safely neglect entropy changes when calculating defect formation energies. In principle, configurational entropy changes should be considered since several individual point defects are required to come together to form a defect cluster. Using the formalism of Korzhavyi *et al.*,[30] we find that the effect of configurational entropy is minor even at 1500 K. For example, in the representative case of a triple defect cluster of $2V_{\mathrm{Ni}}+\mathrm{Ni_{Al}}$, the difference in entropy for the sum of the entropies for two isolated Ni vacancies (V_{Ni}) and an isolated Ni antisite atom ($\mathrm{Ni_{Al}}$) and the entropy for the triple defect ($2V_{\mathrm{Ni}}+\mathrm{Ni_{Al}}$) is small, $T\Delta\Delta S=0.087$ eV at 1500 K. We therefore do not include configurational entropy changes in the following analyses.

Mechanisms consisting of more than one atomic jump are studied stepwise so that a diffusion rate constant is deter-

mined for each step in the form of Eq. (1). The overall activation energy for a multistep mechanism is the energy difference of the highest energy saddle point for the entire mechanism and the initial minimum. Assuming sequential first-order irreversible kinetics, the overall rate of diffusion for a given temperature can be estimated from Eq. (12),

$$\frac{1}{D_{\text{overall}}} = \sum_i \frac{1}{D_i}. \tag{12}$$

Here i is the index representing the step in the mechanism. In order to obtain a pre-exponential factor for comparison to experimental data, the overall diffusion constant for a given temperature is substituted into Eq. (1) along with the overall activation energy in order to solve for an overall D_0.

III. RESULTS AND DISCUSSION

A. Bulk β-NiAl and point defects

Bulk β-NiAl has a CsCl structure consisting of two interpenetrating simple-cubic lattices, one for Ni atoms and one for Al atoms. The lattice parameter is calculated to be 2.896 Å, in good agreement with the experimental value of 2.887 Å.[33] Four types of structural point defects can occur in NiAl: Ni vacancies (V_{Ni}), Al vacancies (V_{Al}), Ni antisite atoms (Ni_{Al}), and Al antisite atoms (Al_{Ni}). A Ni antisite atom consists of a Ni atom on the Al sublattice and vice versa for an Al antisite defect. Experimentally, Ni vacancies and Ni antisite atoms are observed to be the dominant constitutional defects in Al-rich and Ni-rich NiAl, respectively.[33] We confirmed these findings by calculating the defect formation energies of the four point defects, where we predict that the formation energy of a Ni vacancy is smaller than that of an Al antisite (i.e., Ni vacancies are preferred in Al-rich NiAl), whereas we predict Ni antisites have lower formation energies than Al vacancies have (i.e., in Ni-rich NiAl, Ni antisite atoms are preferred).[28] However, since several of the proposed diffusion mechanisms involve Al defects and the temperature range of interest is 1200–1500 K, it is likely that these defects will also be present in NiAl at these high temperatures.

B. Next-nearest-neighbor jumps

The simplest Ni diffusion mechanism one could imagine occurs only on the Ni sublattice. It consists of NNN jumps and requires prior formation of a Ni vacancy, as seen in Fig. 1(a). The saddle point occurs when the Ni atom passes through a plane of four Al atoms. We used a 54-lattice site cell to study this mechanism since increasing the size of the cell to 128-lattice sites did not change (to within 0.01 eV) the formation energy of a Ni vacancy. The MEP [Fig. 1(b)] indicates that the migration energy is 2.58 eV. After adding the Ni vacancy formation energy (0.41 eV) to the migration energy, the overall activation energy is 2.99 eV, in excellent agreement with the experimental value of ~3 eV.[4] Table I gives the entropic factors and pre-exponential factors for 1200 and 1500 K, the range over which experimental data exist. The entropic factor increases the pre-exponential factor

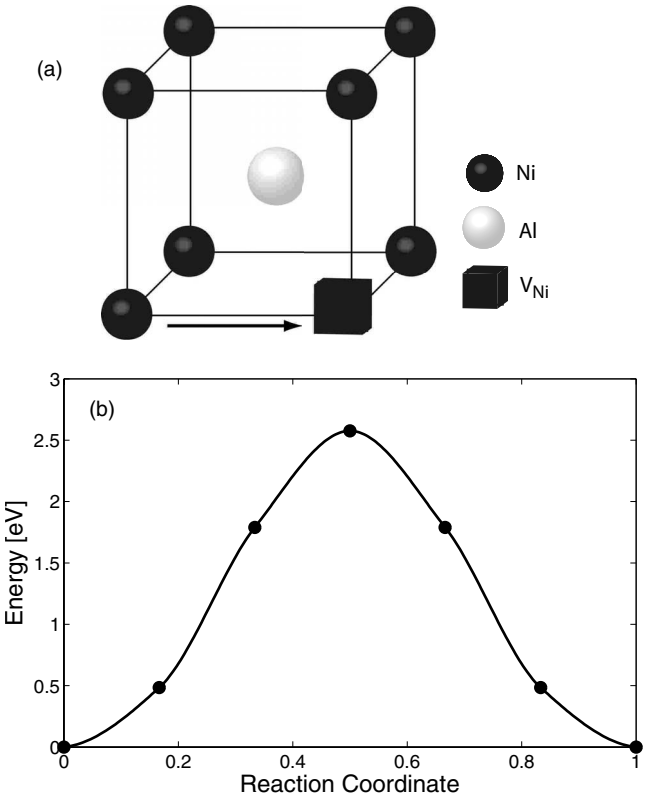

FIG. 1. (a) Diffusion pathway and (b) MEP of a NNN Ni jump.

by more than an order of magnitude, indicating that it would be incorrect to neglect the entropy term in Eq. (8). By including the effect of the entropic barriers, the calculated pre-exponential factors are within a factor of 4 of the experimental value of $\sim 3 \times 10^{-5}$ $\text{m}^2\ \text{s}^{-1}$.[4]

Given that the calculated activation energy and pre-exponential factor agree fairly well with the experimental data, one might conclude that a NNN jump is a viable mechanism for Ni diffusion in NiAl. However, Frank *et al.*[4] concluded the opposite, citing experimental evidence that the activation energy and diffusivity are not affected by the deviation from stoichiometry in Al-rich alloys up to 54% Al. Since Ni vacancies are the dominant constitutional defect in Al-rich NiAl, Frank *et al.*[4] proposed that the rate of diffusion by NNN jumps should have increased in Al-rich NiAl since the formation energy of Ni vacancies would be 0 eV. While we agree that NNN jumps therefore are not the dominant mechanism of Ni diffusion, this mechanism could still play a minor role that simply is not significant enough to change the observed kinetics.

C. Triple defect mechanism

The triple defect mechanism [Fig. 2(a)] was first postulated by Stolwijk *et al.*[34] as a mechanism of diffusion in B2 intermetallics in their work studying diffusion in CoGa. The mechanism consists of four NN jumps initiated by a triple defect cluster comprised in the case of NiAl of two Ni vacancies and a Ni antisite atom. The first step moves the Ni

TABLE I. NNN Ni jump mechanism: migration energies (E_m), activation energies (Q), hTST pre-exponential factors (ν_0), as well as entropic factors and Arrhenius pre-exponential factors (D_0) for 1200 and 1500 K.

			1200 K		1500 K	
E_m (eV)	Q (eV)	ν_0 (THz)	$e^{(-\Delta S/k_B)}$	D_0 (10^5 m^2 s^{-1})	$e^{(-\Delta S/k_B)}$	D_0 (10^5m^2 s^{-1})
2.58	2.99	14.40	25	0.64	32	0.79

antisite atom to a Ni vacancy, creating an Al vacancy and a Ni vacancy. Next, an Al atom moves into the Ni vacancy, leaving a defect cluster of two Al vacancies and an Al antisite atom. The Al antisite atom then moves onto the Al sublattice, recreating a Ni vacancy and an Al vacancy. Finally, a Ni atom moves onto the Al sublattice, leaving the final configuration of a translated Ni triple defect. Through this mechanism, two Ni atoms shift in the same direction by a lattice vector and one Al atom moves by a lattice vector in the opposite direction. A 128-lattice site cell was required to converge the defect formation energies for this mechanism and therefore this was the size of the cell used to study this diffusion pathway.

Previous computational work by Frank *et al.*,[4] using EAM potentials in static lattice simulations, predicted that Ni diffusion in NiAl could occur by this four step mechanism. Our DFT calculations concur, except that we find the mechanism to occur in only three steps. The MEP shown in Fig. 2(b)

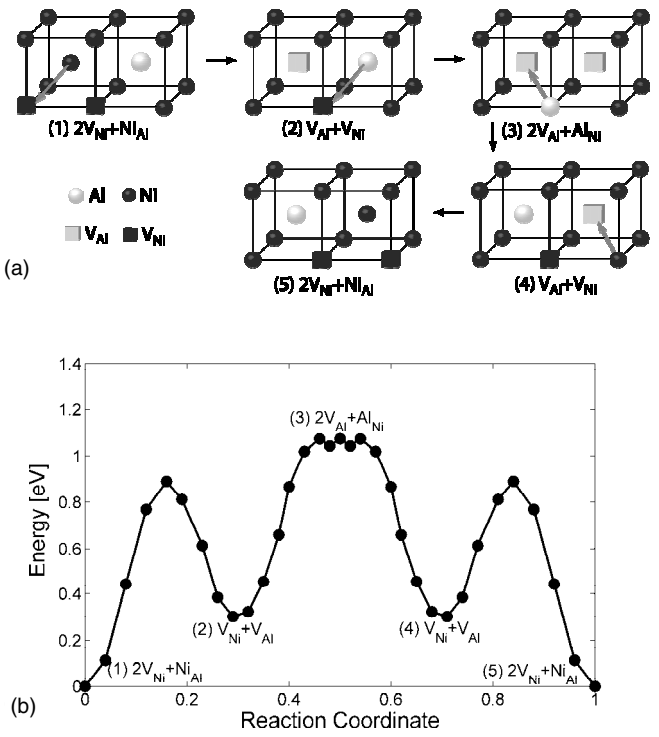

FIG. 2. (a) Diffusion pathway and (b) MEP of the triple defect mechanism, which we predict occurs in three steps: (I) (1)$2V_{Ni}+Ni_{Al} \rightarrow$(2)$V_{Ni}+V_{Al}$, (II) (2)$V_{Ni}+V_{Al} \rightarrow$(4)$V_{Ni}+V_{Al}$, and (III) (4)$V_{Ni}+V_{Al} \rightarrow$(5)$2V_{Ni}+Ni_{Al}$. The oscillation seen in the second step of the MEP is within the uncertainty of the calculations.

indicates that the configuration of two Al vacancies and an Al antisite is a transition state and not a local minimum, contrary to what was predicted via EAM potentials. The calculated normal mode frequencies for the $2V_{Al}+Al_{Ni}$ configuration contain one imaginary frequency ($122i$ cm^{-1}), reaffirming the results of the CINEB calculations. The second step of our predicted mechanism is effectively a NNN Al jump. In order to confirm that no other saddle points are present, we ran a CINEB calculation in which the initial guess for the atomic positions of the diffusing Al atom was simply a linear interpolation between the NNN sites, such that the pathway was not constrained to go through defect cluster 3. The saddle point obtained with this initial guess had exactly the same structure as defect cluster 3, indicating that the Al atom does not take a more direct pathway between Al sites. This is likely due to the presence of the Ni vacancy in clusters 2 and 4; the Al atom prefers to move toward the empty Ni lattice site as it diffuses.

Examining the MEP for the triple defect mechanism in NiAl [Fig. 2(b)], the two images on either side of the saddle-point configuration of $2V_{Al}+Al_{Ni}$ exhibit a slight oscillation in energies around the transition state. The amplitude of the oscillation is only 0.03 eV, which is within the error of the calculations. Therefore, even though we are unable to further resolve the MEP in the region surrounding the transition state, we still can obtain a reliable estimate of the energy barrier. The predicted activation energy for the triple defect mechanism is 3.02 eV [Table II, part (a)], again in excellent agreement with the experimental value. The predicted entropic factors for the triple defect mechanism have a larger effect on the pre-exponential factors than in the case of NNN jumps. The transition state in the triple defect mechanism is more complex than that of a NNN Ni jump, so it is not surprising that the entropic factor makes a larger contribution for the triple defect mechanism due to greater compression of the transition state at 0 K. The agreement between theory and experiment for this mechanism's pre-exponential factor is slightly worse than for the NNN jump but close enough that we cannot exclude this mechanism.

D. Six-jump cycle mechanism

Proposed as a mechanism for diffusion in B2 intermetallics by Elcock and McCombie,[35] the six-jump cycle in principle can occur by three different pathways, one of which results in a Ni atom moving in the [110] direction whereas the other two paths move a Ni atom in the [100] direction. The [110] six-jump cycle [Fig. 3(a)] and the [100] "straight"

TABLE II. Triple defect mechanism: (a) migration energies (E_m), activation energies (Q), and hTST pre-exponential factors (ν_0). (b) Entropic factors and Arrhenius pre-exponential factors (D_0) for 1200 and 1500 K.

(a)

Step	E_m (eV)	Q (eV)	ν_0 (THz)
I	0.89	2.84	3.67
II	0.74	3.00	11.13
III	0.59	2.85	0.66
Overall	1.07	3.02	

(b)

	1200 K		1500 K	
Step	$e^{(-\Delta S/k_B)}$	D_0 (10^5 m^2 s^{-1})	$e^{(-\Delta S/k_B)}$	D_0 (10^5 m^2 s^{-1})
I	116	0.43	145	0.54
II	38	0.56	49	0.70
III	647	0.43	808	0.54
Overall		0.43		0.46

cycle [Fig. 4(a)] consist of six NN jumps occurring in a {110} plane, while three of the jumps in the [100] "bent" cycle [Fig. 5(a)] involve lattice sites out of a {110} plane.[10] All three cycles are proposed to start with a Ni vacancy into

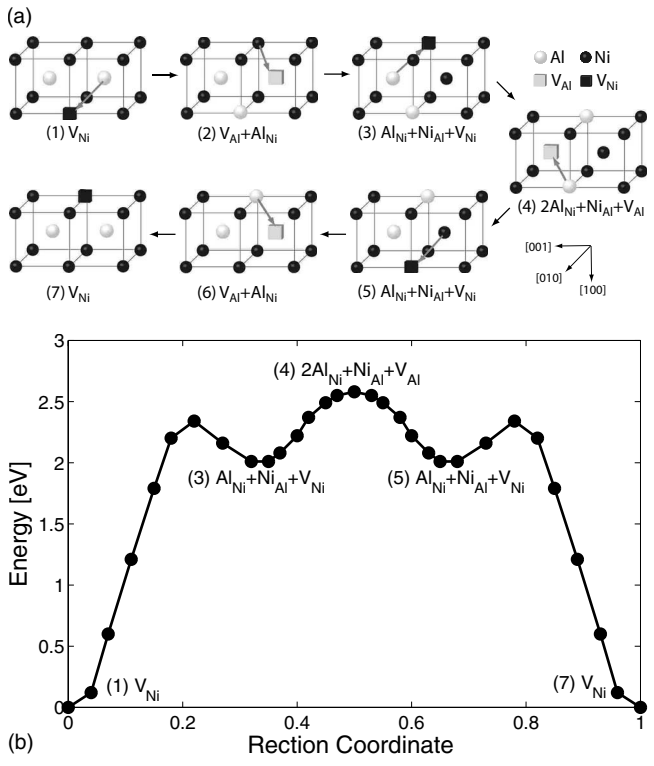

FIG. 3. (a) Diffusion pathway and (b) MEP of the [110] six-jump cycle, which we predict occurs in three steps: (I) (1)V_{Ni} →(3)Al_{Ni}+Ni_{Al}+V_{Ni}, (II) (3)Al_{Ni}+Ni_{Al}+V_{Ni}→(5)Al_{Ni}+Ni_{Al}+V_{Ni}, and (III) (5)Al_{Ni}+Ni_{Al}+V_{Ni}→(7)V_{Ni}.

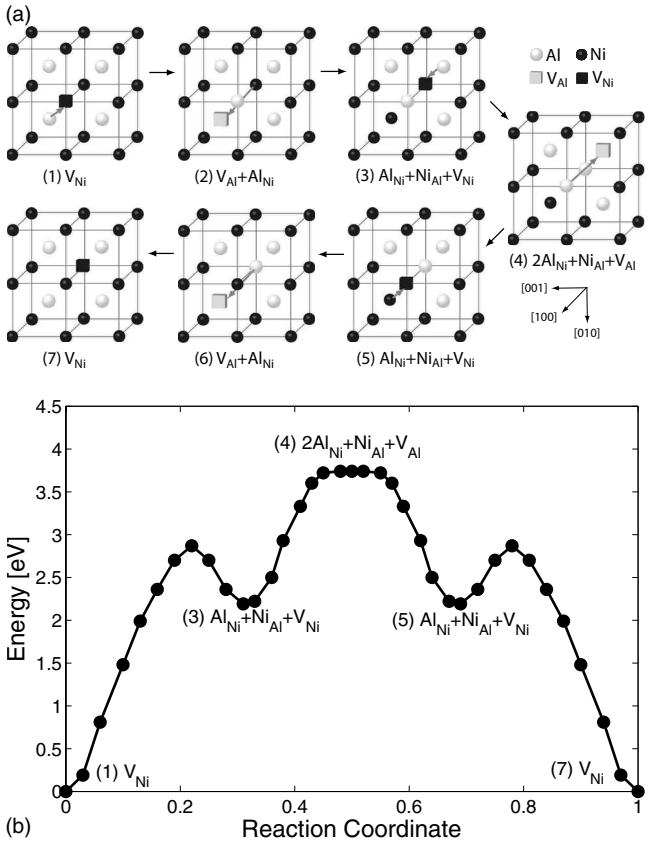

FIG. 4. (a) Diffusion pathway and (b) MEP of the straight [100] six-jump cycle, which we predict occurs in three steps: (I) (1)V_{Ni} →(3)Al_{Ni}+Ni_{Al}+V_{Ni}, (II) (3)Al_{Ni}+Ni_{Al}+V_{Ni}→(5)Al_{Ni}+Ni_{Al}+V_{Ni}, and (III) (5)Al_{Ni}+Ni_{Al}+V_{Ni}→(7)V_{Ni}.

which an Al atom jumps, forming a defect cluster of an Al vacancy and an Al antisite atom. Then a Ni atom moves into the Al vacancy creating a defect cluster of an Al antisite, a Ni antisite, and a Ni vacancy. An Al atom fills the Ni vacancy forming a cluster of two Al antisites, a Ni antisite, and an Al vacancy. Because of symmetry, the second half of the cycle consists of the same NN jumps but in reverse order.

When we attempted to calculate the defect formation energy of the V_{Al}+Al_{Ni} defect cluster, the Al atom relaxed back to the Al sublattice and created a Ni vacancy instead. This indicates that this proposed intermediate is not stable.[28] Since Al vacancies and antisites are not typically found in NiAl,[33] it is understandable that a complex of both defects would be much less stable than a Ni vacancy. Consequently, the first two jumps were combined in the CINEB calculations so that the Al and Ni atoms move at the same time. This concerted motion is possible because the Ni atom takes the place of the Al atom which is moving away from the Ni atom. The symmetry of this mechanism dictates that the fifth and sixth jumps for all three six-jump cycles also are combined. As a result, we predict that the maximum number of jumps that can occur in six-jump cycle is actually only four. In order to distinguish between the postulated mechanism and our calculated pathway, roman numerals will be used when referring to our steps in the mechanism.

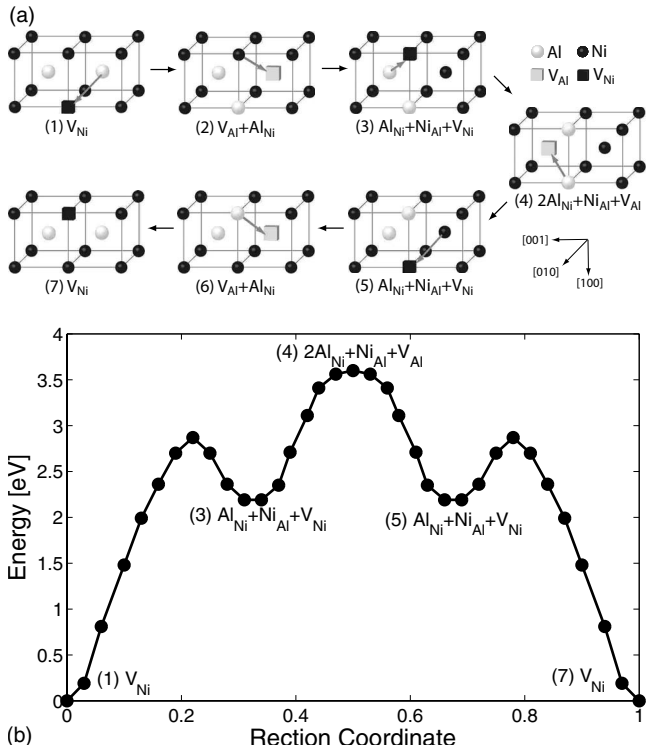

FIG. 5. (a) Diffusion pathway and (b) MEP of the bent [100] six-jump cycle, which we predict occurs in three steps: (I) (1)V_{Ni} $\rightarrow$(3)Al_{Ni}+Ni_{Al}+V_{Ni}, (II) (3)Al_{Ni}+Ni_{Al}+$V_{Ni}$$\rightarrow$(5)$Al_{Ni}$+$Ni_{Al}$+$V_{Ni}$, and (III) (5)$Al_{Ni}$+$Ni_{Al}$+$V_{Ni}$$\rightarrow$(7)$V_{Ni}$.

1. [110] six-jump cycle

The CINEB calculations reveal that the [110] six-jump cycle actually occurs in only three jumps [Fig. 3(b)]. We predict from the MEP that the defect cluster of 2Al_{Ni}+Ni_{Al} +V_{Al} is actually a transition state and not a local minimum as originally postulated. The normal mode frequencies calculated for this defect cluster resulted in one imaginary frequency, reaffirming this conclusion. Using an EAM potential in NEB calculations, Mishin *et al.*[10] also concluded that this pathway occurred in three steps not six. Regarding the combined motion of the Ni and Al atoms in step I, the Ni atom does not move very far from its initial position until the Al atom is very close to its final position, so this step is only slightly concerted.

The activation energy for this mechanism (Table III) is once again in line with the experimental value (2.99 eV vs $\sim$3 eV), indicating that the [110] six-jump cycle is a plausible mechanism for Ni diffusion in NiAl. Similar to the triple defect mechanism, the entropic factor increases the pre-exponential factor by several orders of magnitude, as would be expected since the defect clusters consist of as many as four point defects. Additionally, the calculated pre-exponential factor is essentially the same as that calculated for the NNN Ni jump, which is within a factor of 4 of the experimental value of $\sim 3\times 10^{-5}$ m^2 s^{-1}. Thus, the [110] six-jump cycle is a viable mechanism for Ni diffusion in NiAl.

TABLE III. [110] six-jump cycle mechanism: (a) migration energies (E_m), activation energies (Q), and hTST pre-exponential factors (ν_0). (b) Entropic factors and Arrhenius pre-exponential factors (D_0) for 1200 and 1500 K.

(a)

Step	E_m (eV)	Q (eV)	ν_0 (THz)
I	2.34	2.75	0.30
II	0.56	2.97	0.78
III	0.33	2.74	3.06
Overall	2.58	2.99	

(b)

	1200 K		1500 K	
Step	$e^{(-\Delta S/k_B)}$	D_0 (10^5 m^2 s^{-1})	$e^{(-\Delta S/k_B)}$	D_0 (10^5 m^2 s^{-1})
I	140	1.47	174	1.83
II	545	0.57	682	0.72
III	1449	1.47	1811	1.83
Overall		0.64		0.74

2. Straight [100] six-jump cycle

This pathway can be ruled out as a possible mechanism for Ni diffusion in NiAl since the calculated activation energy is much higher than experiment, as shown in Table IV. The migration energy itself is almost 3.75 eV, and when the formation energy of a Ni vacancy is added in, the total activation energy is 4.14 eV, more than 1 eV higher than the experimental value. The high value for the migration energy is most likely due to the close proximity of the antisite defects, especially in the 2Al_{Ni}+Ni_{Al}+V_{Al} cluster, where the two Al antisite atoms are NNNs. These NNN antisite Al atoms are also NN to two other Al atoms [see Fig. 4(a), intermediate (4)]. Since Al is the larger atom in NiAl, such a cluster of Al atoms creates considerable strain on the lattice.

The migration energy for step I is $\sim$0.5 eV higher in the straight [100] cycle than in the [110] cycle. In the latter cycle, the Ni vacancy into which the Al atom is to move is a third NN of the Ni atom that takes the place of the Al atom. In the straight [100] cycle, the Ni vacancy and Ni atom are NNNs, leading to movement of Al and Ni atoms that are closer than the same atoms in the [110] cycle, creating more strain on the lattice.

From the MEP it appears that this mechanism occurs in three steps and the 2Al_{Ni}+Ni_{Al}+V_{Al} defect cluster is a saddle point. We were unable to confirm this with frequency calculations because no imaginary frequencies were found for this cluster, even when the displacement used to calculate the Hessian was increased to 0.03 Å. Since the smallest frequency (37 cm^{-1}) is below 50 cm^{-1}, we hesitate to classify this structure as a local minimum or a saddle point. For the initial CINEB calculations, a band was strung between defects 3 and 4 [Fig. 4(a)] to generate the MEP [Fig. 4(b)] for the first half of step II, generating the second half using

TABLE IV. Bent (B) and straight (S) [100] six-jump cycle mechanisms: (a) migration energies (E_m), activation energies (Q), and hTST pre-exponential factors (ν_0). Steps I and III are equivalent for both bent and straight mechanisms. (b) Entropic factors and Arrhenius pre-exponential factors (D_0) for 1200 and 1500 K.

(a)

Step	E_m (eV)	Q (eV)	ν_0 (THz)
I	2.87	3.28	16.5
II (B)	1.41	4.00	2.67
II (S)	1.55	4.14	[a]
III	0.68	3.27	0.84
Overall (B)	3.60	4.01	
Overall (S)	3.74	4.15	

(b)

	1200 K		1500 K	
Step	$e^{(-\Delta S/k_B)}$	D_0 (10^5 m^2 s^{-1})	$e^{(-\Delta S/k_B)}$	D_0 (10^5 m^2 s^{-1})
I	26	1.58	32	1.98
II (B)	160	1.11	200	1.39
III	506	1.58	634	1.98
Overall (B)		1.21		1.49

[a]The pre-exponential factors for step II of the straight jump could not be calculated due to the nature of the potential-energy surface at the saddle point.

symmetry. In hope of resolving the saddle-point dilemma, we then performed a CINEB calculation between defects 3 and 5. The saddle point for this longer band has the same structure as that found by minimizing the total energy of the $2Al_{Ni}+Ni_{Al}+V_{Al}$ defect cluster. Since we have ruled out this mechanism as contributing to Ni diffusion in NiAl, no further investigation of this point was completed. We can postulate that the $Al_{Ni}+Ni_{Al}+V_{Al}$ cluster is either a saddle point or a minimum in a very shallow well on the potential energy surface. As a result of the ambiguity at the saddle point, we have not calculated pre-exponential factors for step II.

3. Bent [100] six-jump cycle

The difference in the bent and straight [100] six-jump cycles lies in the structure of the third intermediate [labeled (4) in Fig. 5(a)]. In contrast to the straight [100] six-jump cycle, we were able to confirm that the $2Al_{Ni}+Ni_{Al}+V_{Al}$ defect cluster is a saddle point since one imaginary frequency ($58i$ cm^{-1}) was found at this point. The MEP [Fig. 5(b)] for steps I and III is the same for both [100] jumps, and the 0.14 eV difference in activation energies is due to the difference in the migration barrier of step II. The $Al_{Ni}+Ni_{Al}+V_{Al}$ defect is more spread out in the straight cycle than in the bent cycle creating more strain on the lattice, so the migration energy for step II is slightly less for the bent cycle. Again, the high overall migration energy is probably a result of the crowding of the two Al antisite defects in the same manner as the straight [100] cycle. As in the [110] six-jump cycle, we predict the bent [100] mechanism actually occurs in only three steps. Since the total activation energy is 4 eV, we can rule out this mechanism as contributing to diffusion.

TABLE V. Comparison of the calculated activation energies and pre-exponential factors with experimental values in the literature for $1050 \leq T \leq 1630$ K.

Mechanism	Q (eV)	D_0 (10^5 m^2 s^{-1}) 1500 K
NNN	2.99	0.79
Triple defect	3.02	0.46
Six jump [110]	2.99	0.74
"Bent" six jump [100]	4.01	1.49
"Straight" six jump [100]	4.15	[a]
Experiment[b]	2.99, 3.01, 2.97	2.71, 3.45, 2.77

[a]We were unable to calculate a value due to a lack of imaginary frequency at the saddle point.
[b]Reference 4.

Using molecular dynamics with EAM potentials to study Ni diffusion in NiAl, Soule de Bas and Farkas[9] found that the dominant diffusion mechanism was the [110] six-jump cycle. The percentage of [100] jumps, if they were seen at all, was quite low.[9] These observations are in line with our findings since the activation energy of a [110] jump is ~1 eV less than for both the straight and bent [100] jumps. In their MD simulations, NNN Ni jumps contributed negligibly to diffusion. As noted by Krachler and Ipser,[36] since Soule de Bas and Farkas[9] chose to begin their simulations with a single Ni vacancy, it would not have been possible for the triple defect mechanism to occur, so unfortunately, they were not able to make a decisive ruling on whether the [110] six-jump cycle or the triple defect mechanism dominates. Using static lattice simulations with EAM potentials, Mishin *et al.*[10] also found higher migration energies for the [100] cycles compared to the [110] cycle. Additionally, they identified the defect cluster of $2Al_{Ni}+Ni_{Al}+V_{Al}$ to be a local minimum in the [100] cycles, whereas we predict it to be a saddle point for the bent [100] mechanism. While qualitatively their results agree with ours, we predict lower migration energies, which should be more accurate due to the nonempirical nature of DFT and its inherent relatively high accuracy for metallic systems.

IV. CONCLUSIONS

We have used first-principles calculations to test postulated mechanisms for Ni diffusion in NiAl. When comparing our calculated activation energies and pre-exponential factors with experimental data (Table V), these calculations show that NNN jumps, the triple defect mechanism, and the six-jump cycle mechanism in the [110] direction initially are all plausible mechanisms for Ni diffusion in stoichiometric NiAl since all three exhibit quantitative agreement with measured diffusion kinetics parameters. We have ruled out the [100] direction six-jump cycle mechanisms (bent and straight) for

Ni diffusion since the calculated activation energies are ~1 eV higher than experiment. The significantly larger activation energy for the [100] six-jump cycle mechanisms can be attributed to the differences in structure and stability of the transition states in step II of the [110] and [100] six-jump cycles ($2Al_{Ni}+Ni_{Al}+V_{Al}$). In the latter, the two Al antisite atoms are closer together than in the [110] cycle, creating larger strain in the lattice and thereby raising the activation energy of the transition states for the [100] cycles.

The experimental data of Frank *et al.*[4] show that the activation energy and diffusivity of Ni diffusion in NiAl remain relatively constant in the Ni concentration range of 46–50 at. %, which they interpreted to indicate that the same diffusion mechanisms operating in stoichiometric NiAl are responsible for Ni diffusion in the Al-rich regime. Since all three mechanisms have initial and final minima involving Ni vacancies, this is plausible because the dominant structural defects in Al-rich NiAl are Ni vacancies. However, Frank *et al.*[4] expected (but did not observe) an increase in Ni diffusivity in Al-rich NiAl since Ni vacancies are naturally present (i.e., no cost to form Ni vacancies is incurred), and therefore the activation energy simply would be equal to the migration energy. Since an increase in Ni diffusivity was not observed, Frank *et al.*[4] ruled out the NNN Ni jump and six-jump cycle mechanisms which begin and end with a Ni vacancy. Although we agree that NNN Ni jumps should be excluded [also because the NNN jump distance is larger than all NN jumps in the other mechanisms], the case of the six-jump cycle is less clear. A mechanism consisting of three steps may not always occur smoothly and irreversibly starting with the initial minimum. In a real alloy at the temperatures for which the experimental data are collected, not all cycles will be completed and a mechanism could begin from an intermediate state. Therefore it is plausible that the [110] six-jump cycle could contribute to diffusion of Ni in NiAl.

In Ni-rich NiAl, the diffusivity of Ni has been measured to increase as the concentration of Ni increases from stoichiometry, indicating that other mechanisms than those studied here may be operating.[4] Since the dominant constitutional defects in Ni-rich NiAl are Ni antisites, the ASB mechanism has been postulated,[37] which operates via Ni atoms on both the Ni and Al sublattice. Since the bond coat of thermal barrier coatings will be Ni rich, the ASB mechanism may be an important contributor to Ni diffusion in TBCs; we will examine this mechanism and the effect of Pt on it in future work.

Our ultimate goal is to examine the effect of Pt on Al diffusion in NiAl using the postulated Ni diffusion mechanisms as a basis for studying possible Al pathways. Even though no experimental data for Al diffusion in NiAl exist to compare with theory, we are confident based on the current quantitative agreement with Ni diffusion measurements that our future study of Al diffusion will provide valid conclusions about Al diffusion in NiAl. Already we can infer some information based on our results for Ni diffusion in NiAl. An analogous pathway to the Ni triple defect mechanism beginning with an Al triple defect ($2V_{Al}+Al_{Ni}$) will not occur since this defect complex is a saddle point and not a local minimum like the Ni triple defect ($2V_{Ni}+Ni_{Al}$). The triple defect mechanism of Ni diffusion does lead to propagation of Al atoms [see Fig. 2(a)], and since we predict this mechanism to contribute to Ni diffusion, it must contribute to Al diffusion simply in the opposite direction from Ni diffusion. The six-jump cycles do not result in long-range Al transport, but it would be possible to propose an analogous mechanism to the three six-jump cycles beginning with an Al vacancy. We currently are examining the effects of Pt on Ni and Al diffusion to fulfill our overall goal of predicting why Pt has a beneficial effect on TBC lifetime.

ACKNOWLEDGMENTS

We are grateful to the (U.S.) Air Force Office of Scientific Research for funding and Maui High Performance Computing Center and Naval Oceanographic Office and Engineering Research and Development Center Major Shared Resource Centers for computing time.

[1] I. G. Wright and B. A. Pint, Proc. Inst. Mech. Eng., Part A **219**, 101 (2005).
[2] G. W. Goward, Surf. Coat. Technol. **108**, 73 (1998).
[3] N. P. Padture, M. Gell, and E. H. Jordan, Science **296**, 280 (2002).
[4] S. Frank, S. V. Divinski, U. Sodervall, and C. Herzig, Acta Mater. **49**, 1399 (2001).
[5] G. F. Hancock and B. R. McDonnell, Phys. Status Solidi A **4**, 143 (1971).
[6] S. V. Divinski and C. Herzig, Intermetallics **8**, 1357 (2000).
[7] S. V. Divinski, S. Frank, C. Herzig, and U. Sodervall, Solid State Phenom. **72**, 203 (2000).
[8] G. Chen, J. Zhang, and K. Xu, J. Alloys Compd. **430**, 102 (2007).
[9] B. Soule De Bas and D. Farkas, Acta Mater. **51**, 1437 (2003).
[10] Y. Mishin, A. Y. Lozovoi, and A. Alavi, Phys. Rev. B **67**, 014201 (2003).
[11] Q. Xu and A. Van der Ven (unpublished).
[12] G. Kresse and J. Furthmüller, Comput. Mater. Sci. **6**, 15 (1996).
[13] G. Kresse and J. Furthmüller, Phys. Rev. B **54**, 11169 (1996).
[14] P. Hohenberg and W. Kohn, Phys. Rev. **136**, B864 (1964).
[15] W. Kohn and L. J. Sham, Phys. Rev. **140**, A1133 (1965).
[16] J. P. Perdew, K. Burke, and M. Ernzerhof, Phys. Rev. Lett. **77**, 3865 (1996).
[17] J. P. Perdew, J. A. Chevary, S. H. Vosko, K. A. Jackson, M. R. Pederson, D. J. Singh, and C. Fiolhais, Phys. Rev. B **46**, 6671 (1992).
[18] P. E. Blöchl, Phys. Rev. B **50**, 17953 (1994).
[19] G. Kresse and D. Joubert, Phys. Rev. B **59**, 1758 (1999).
[20] M. Methfessel and A. T. Paxton, Phys. Rev. B **40**, 3616 (1989).
[21] H. J. Monkhorst and J. D. Pack, Phys. Rev. B **13**, 5188 (1976).
[22] F. D. Murnaghan, Proc. Natl. Acad. Sci. U.S.A. **30**, 244 (1944).
[23] G. H. Vineyard, J. Phys. Chem. Solids **3**, 121 (1957).
[24] G. Henkelman, B. P. Uberuaga, and H. Jonsson, J. Chem. Phys.

113, 9901 (2000).
[25] C. Zener, J. Appl. Phys. **22**, 372 (1951).
[26] Y. Mishin, M. D. Sorensen, and A. F. Voter, Philos. Mag. A **81**, 2591 (2001).
[27] H. B. Huntington, G. A. Shirn, and E. S. Wajda, Phys. Rev. **99**, 1085 (1955).
[28] K. A. Marino and E. A. Carter, Acta Mater. **56**, 3502 (2008).
[29] C. Jiang, M. F. Besser, D. J. Sordelet, and B. Gleeson, Acta Mater. **53**, 2101 (2005).
[30] P. A. Korzhavyi, A. V. Ruban, A. Y. Lozovoi, Y. K. Vekilov, I. A. Abrikosov, and B. Johansson, Phys. Rev. B **61**, 6003 (2000).
[31] B. Meyer and M. Fähnle, Phys. Rev. B **59**, 6072 (1999).
[32] K. A. Marino and E. A. Carter (unpublished).
[33] D. B. Miracle, Acta Metall. Mater. **41**, 649 (1993).
[34] N. A. Stolwijk, M. van Gend, and H. Bakker, Philos. Mag. A **42**, 783 (1980).
[35] E. W. Elcock and C. W. McCombie, Phys. Rev. **109**, 605 (1958).
[36] R. Krachler and H. Ipser, Phys. Rev. B **70**, 054113 (2004).
[37] C. R. Kao and Y. A. Chang, Intermetallics **1**, 237 (1993).